Comparative Characterization of Melt Electrospun Fibers and Films Based on PLA-PHB Blends: Diffusion, Drug Release, and Structural Features

*Yong Liu, Kuan Cao, Svetlana Karpova, Anatoliy Olkhov, Anna Filatova, Anna Zhulkina, Andrey Burkov, Sergey V. Fomin, Derval S. Rosa, and Alexey L. Iordanskii**

Comparative structural-dynamic characterization of the biopolyester blends based on poly(3-hydroxybutyrate) and poly-L-lactide (PLA) [PHB/PLA] is performed. The melt electrospun fibers and molded films with the same compositions (1/0, 1/9, 3/7) but obtained by two different fabrication ways are explored by combination of structural and dynamic methods. The structural-dynamic features such as segmental mobility (by spin-probe ESR technique), thermophysical transitions (by DSC), and surface morphology (by SEM) are applied to elucidate the distinctive diffusion features as the essential constituent of drug release. The ultrathin electrospun fibers and molded films loaded by dipyridamole (DPD), as a modeling drug, shows the different structural behavior including crystallinity and the diversity in diffusion coefficients and the drug release profiles. To emphasize the special transport phenomena in nano-sized drug vehicles, the diffusivity modeling is performed and further the drug diffusion coefficients in the ultrathin fibers and the macroscopic films are compared.

1. Introduction

Elaboration of contemporary therapeutic systems for drug delivery is based on both the comprehensive application of novel bio-based polymers composites and the study on diffusion-degradation temporary-spatial patterns. It is difficult to overestimate the impact of polymer structure and morphology upon drug immobilization and drug diffusivity that is confirmed by the wide spectrum of the biodegradable polymer applications in the different areas of biomedicine such as tissue engineering, development of multifunctional implants, fabrication of surgery threads, targeted drug therapy, and others.[1–3] The appliance of polymer therapeutic units pertaining to the diverse categories from macroscopic implants to nanoparticles enables the experts to give the immediate opportunity for price reducing in expensive medicines, a toxicity decrease, and, most importantly, for addressing a "drug-bullet" to a "tissue-target."[4]

Biodegradable polyester category is a unique family of biomedical plastic materials which has disclosed the comprehensive concept in drug formulation industry. The polyesters namely polylactides [PLA], polyglycolides, poly(ε-caprolactone), poly(3-hydroxybutyrate) [PHB], and their copolymers or blends are a well-known option for drug-vehicles performance.[5,6] In the majority, these polymers have the unique characteristics such as tailoring of degradation rates, drug transport controlling, minimal immune response, and extremely low toxicity that make them as coherently prominent materials for biomedical applications and especially for the design of drug delivery therapeutic systems.

More often than not, drug diffusion in polymer matrices manifests itself as an inherent process determining the drug movement in polymer vehicles and in combination with other coherent processes such as polymer swelling, polymer dissolution, and macromolecular degradation determines the mechanism and drug delivery profile evolution.[7–8] Because the drug release profiles determine the functional behavior and efficacy of polymer therapeutic systems, special accent will be provided to compare the release characteristics as the function of geometry

Y. Liu, K. Cao
Beijing Key Laboratory of Advanced Functional Polymer Composites
Beijing University of Chemical Technology
Beijing 100029, China

S. Karpova
Emanuel Institute of Biochemical Physics
Kosygin Str. 4, Moscow 119991, RF

A. Olkhov, A. Filatova, A. Zhulkina, A. L. Iordanskii
Semenov Institute of Chemical Physics
Kosygin Str. 4, Moscow 119991, RF
E-mail: aljordan08@gmail.com

A. Burkov, S. V. Fomin, A. L. Iordanskii
Vyatskiy State University
Moskovskaya ul. 36, Kirov (obl.) 610000, RF

D. S. Rosa
Universidade Federal do ABC (UFABC)
. Av. dos Estados, 5001, Santo André, Sao Paulo, Brazil

The ORCID identification number(s) for the author(s) of this article can be found under https://doi.org/10.1002/masy.201800130.

DOI: 10.1002/masy.201800130

and diffusion features of modeling drug release especially under conditions of initial stage of degradation development.

The purpose of this manuscript is to conduct the comparative analysis of drug diffusion (DPD) based on diffusivity impact upon general process of release. In a sense, the content outlined here presents the development of our recently published data on the ecologically friendly, melt electrospinning technology of nanofibers for drug delivery.[9] Here we have used the melt-spun ultrathin fibers on the base of PLA/PHB compositions and simultaneously the analogous films produced via a melt moulding under the analogous temperature conditions. Additionally the structure and dynamic characteristics of these biopolymer vehicles have been represented, that should clarify the drug release features in polymer therapeutic systems of different geometry, namely macro- and submicron specimens.

2. Experimental Section

2.1. Materials

PHB (1001MD, BASF) and PLA particles ($M_n = 100\ 000$; Zhejiang Hisun Biomaterials Co., Ltd., China) were dried at 60 °C for 6 h in a vacuum oven before the experiments. Dipiridamole (DPD) ($M_w = 504.63$; >98.0%) was purchased from Beijing Inoke Technology Co. Ltd., China.

2.2. Processing of the Blends for Electrospinning

Blends of PLA and PHB at different PLA/PHB ratios of 1/0 (PLA) 9/1, 7:3, 0/1 (PHB) by weight were mixed in a Haake polylab torque rheometer at 190 °C for 6 min at a constant rotor speed of 80 rpm. The PLA/PHB ratios of 9:1 and 7:3 with 1% and 5% DPD by weight are the same condition except for the temperature at 170 °C.

2.3. Processing of the Films

The powders with different PLA/PHB ratio (1/0, 9/1, 7/3) and mixed with 1 and 5 wt% dipyridamole were molded into the films (thickness = 80 ± 4 μm) along the vertical direction at 177 °C and 10 KPa for 5 min using a Carver Laboratory Press (Model C). The press was pre-heated at 150 °C and then the PLA/PHB + xDPD ($x = 1.5\%$) powder was placed in a stainless steel frame with top and bottom covers (50 × 50 × 1.0 mm). To prevent the moulded film adhesion to the metal surface and facilitate sample detaching, the polyimide films (Kapton, DuPont) were used.

2.4. Melt Electrospinning

The melt electrospinning devices used are the same as in our previous studies.[10] The collector covered with aluminum foil was connected to the positive of the power, and the spinneret was grounded. Samples were prepared using a normal power supply (DW-P503-2ACDE; Dong Wen high-voltage power supply (Tianjin) Co., Ltd., China). First, several electrospinning processing conditions were tried to produce the electrospinning fiber of PLA and the ratio of 9:1. The different positive voltages, applied cylinder temperature, spinning distance were investigated for the formation of a stable Taylor cone to obtained uniform and continuous fiber. Because of the addition of the DPD, the applied temperatures could be decreased notably, and it was fixed to 170 °C. The DPD acts as the plasticizer in melt electrospinning and decreases polymer-polymer interaction to make segments of polymer move at low temperature.[25] Thus the melt electrospinning was carried out at 220 °C without DPD and 170 °C with DPD, the applied voltage was 35 kV, and the distance between collector and spinneret was set at 7 cm.

2.5. Characterization

Electrospun fiber mats were coated with Au and their morphology was characterized using scanning electron microscopy (SEM, Hitachi S4700, Japan) with an accelerating voltage of 20 kV. The average fiber diameter and its size distribution were calculated using SEM images by Image J software. Over approximately 20 fibers of each sample were randomly selected from the SEM image, and each fiber was measured at five different locations. Thermophysical characteristics and crystallization behavior were obtained by Differential scanning calorimetry (DSC Q20 TA Instruments, USA) with the samples being heated from 0 to 200 °C at 10 °C min^{-1} under a nitrogen atmosphere (20 mL min^{-1}). The glass transition temperature (Tg), cold crystallization temperature (Tcc), melting temperature (Tm), and crystallization temperature (Tc) were obtained from the first heating and crystallinity degree X_C (%) was calculated using standard equation[11]:

$$X_c = (\Delta H_m - \Delta H_c)/(\Delta H_f \cdot w_{PLA})$$

where ΔH_f is the melting heat associated with pure crystalline PLA (93 Jg^{-1})[12] and w_{PLA} is the weight fraction of PLA in the blend.

Segmental mobility of PLA and PHB in the blend fibers was studied by probe electron spin-resonance spectroscopy (ESR) method. X-band EPR spectra were registered on an automated EPR-V spectrometer (Semenov Institute of Chemical Physics, Moscow RF.). A stable nitroxide radical TEMPO (2,2,6,6-tetramethylpyperidin-1-oxil) was used as a spin-probe. The radical was introduced into the fibers from the gas phase at 40 °C. The radical concentration in the polymer was not above 10^{-3} mol L^{-1}. The experimental spectra of the spin probe in the region of slow motions ($\tau > 10^{-10}$ s) were analyzed within the model of isotropic Brownian rotation using a special program described in ref. [13]. The spectra were modeled using the following main values of the g-tensor and the hyperfine coupling tensor of the radical: $g_{xx} = 2.0096$, $g_{yy} = 2.0066$, $g_{zz} = 2.0025$, $A_{xx} = 7.0$G, $A_{yy} = 5.0$ G, and $A_{zz} = 35.0$ G. The value A_{zz} was determined experimentally from the EPR spectra of the nitroxide radial in the polymer at −216 °C; it was almost equal to the values Timofeev et al.[14] reported. The correlation time of probe rotation, τ, were determined from the ESR spectra via the equation[15]:

$$\tau = \Delta H^{+} \times \left[(I^{+}/I^{-})^{0.5} - 1 \right] 6.65 \times 10^{-10} [S],$$

where ΔH^{+} is the width of spectrum component located in a weak field and I^{+}/I^{-} is the ratio of component intensities in weak and strong fields of the spectrum, respectively. The statistical error of τ measurements is equal to ± 5.

The DPD release from the PHB films and the fibrillar mats was carried out as follows: a rectangular fragment cut out from the prepared films (≈10 mg) were suspended in 50 mL of phosphate buffer medium (pH = 7.4 ± 0,2) at 25 °C under continuous stirring at a moderate speed of 200 rpm in a thermostatically controlled glassy cell. To estimate the amount of drug released into aqueous medium, 3 cm^3 of test aliquot was drawn off with the pipette in specified time intervals and analyzed by UV–VIS spectrometer at the wavelength equals to 292 nm that corresponds to the maximal absorption band of DPD. For every aliquot removed, the same quantity of fresh water/buffer was added. Each measuring was repeated threefold and the averaged value has been used as one experimental point. The kinetics of DPD release was studied with Beckman DU-65 UV spectrophotometer (USA). The interval of sampling depended on the fiber composition and, accordingly, on the rate of drug release; it was from 1 to 30 min. The experiments lasted from several hours to several days.

3. Results and Discussion

3.1. Surface Morphological Patterns

The surface morphology of a single filament which is typical for PLA/PHB/DPD blend nanofibers (9/1 + 1% DPD) and the surface pattern of the PHB/PLA/DPD blend film are shown in **Figure 1** (A and C, respectively) for the comparison. Additionally, the AFM image of the same single fiber is presented in Figure 1B. Both micrographs (A,C) obtained by different techniques indicate that the melt-electrospun nanofibers with the PHB/PLA blend ratio 1:9 have a uniform structure without any features of cylindrical form deformation. Additionally, the surface of filaments is quite perfect and has not visible cracks and pores. Almost at the same SEM magnification the surface of the molded films with the analogues PHB/PLA proportion looks lightly structured with uneven Pt-shading density that corresponds to the alternation of petty bulges and notches.

In our previous paper[9] it was reported, that the PHB loading to PLA matrix decreases the mean fiber diameter from 20.0 ± 2.5 μm at the 9:1 ratio to 18.8 ± 2.5 μm at the 7:3 ratio and finally to 10.6 ± 2.5 μm at the PLA/PHB ratio equals to 6:4. The drug embedding in the polymer system decreases the mean fiber diameter up to 10.7 ± 2.5 μm for 7:3 +1% DPD system and simultaneously leads to narrower diameter distribution. As it can show in Figure 1A,B the averaged diameters of the fibers coincide well with the newly obtained results on the diameter dimensions which are equal to ≈10 μm and 12.2 μm respectively obtained by SEM and AFM techniques.[16]

The variance in structure-morphology characteristics of polymer fibers obtained via classical solvent electrospinning and corresponding films obtained via solution casting could be explained by the discrepancy in the formation conditions and primarily by the difference of solvent evaporation conditions. In framework of diffusion model, the rate of solvent desorption from an ultrathin cylindrical filament with diameter about 100 nm (10^{-7} m) and from the surface of a plane macroscopic film with the thickness equals to about 100 μm (10^{-4} m) should differ by as much as six order. For instance, in the work[17] it was stated that for the nanofibers under electrospinning conditions the time of desorption should take several millisecond, while solvent evaporation from the films with analogous content is gradually performed for essentially longer time, namely dozens of hours and even more.

In event of melt electrospinning and subsequent comparison of the spun fibers with the macroscopic molded films, the differences in the conditions of their production are not so obvious and related to heat dissipation more likely, that is, by cooling specification of fibers and films. It is quite difficult to describe the differences in temperature gradients for the formation of fibers and films from a melt and such description

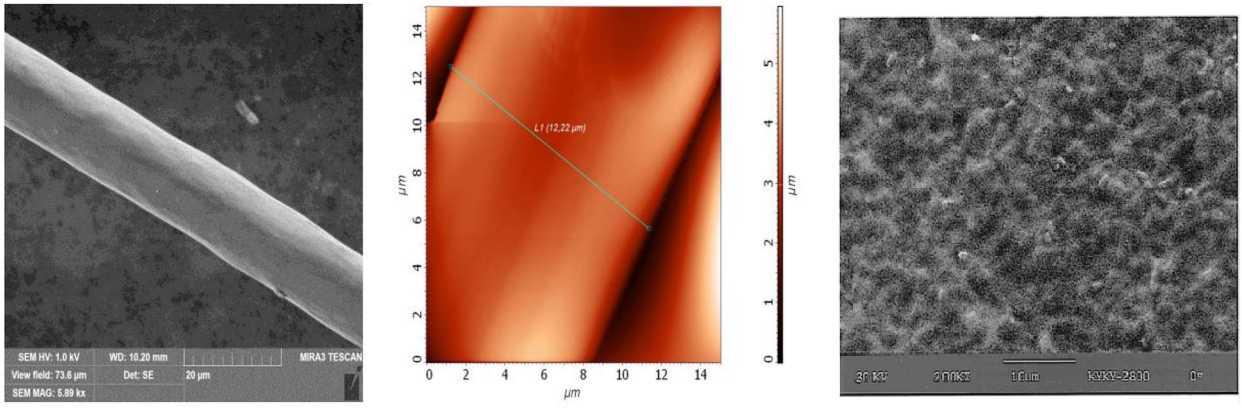

Figure 1. Surface morphology and diameter histograms of melt-electrospun ultrathin fibers with PLA/PHB ratio 9:1 (A,C) and 7:3 (D), and melt-pressed PLA/PHB film (9:1) (B).

is not included in this paper content. Nevertheless, it is possible to assume that melt electrospinning without solvents leads to the formation of the smooth surfaces of nanofibrils that is confirmed by both SEM and AFM images in Figure 1A,B, respectively. On the contrary, according to the comprehensive work of Megelski et al.[17] in the polystyrene fibers the presence of volatile solvents affects dramatically surface morphology due to pore formation.

In absence of through-going or deeply extended pores the lightly roughened surface should not practically affect on the interior drug diffusion but could alter the diffusion boundary conditions. The surface roughness evolution of PLA and PHB during the hydrolysis has been described in our preliminary work.[18]

3.2. Thermal Data for PLA PHB Fibers and Films

Thermal phenomena in biodegradable polymers, especially such as melting, crystallization, and vitrification, determine the physical state of a polymer matrix, the ratio between amorphous and crystalline phases, and, hence promote the coherent option for their description of mechanical, hydrolytic, and diffusion behavior. To compare the thermal characteristics for PLA, PHB, and their blends prepared in the forms of films and fibers, the thermograms obtained by the DSC technique have been obtained and collected in Table1.

The DSC curves of the initial heating PLA/PHB for the films at the ratio 9/1/1 (A) and the corresponding curves for the ultrathin fibers with the 9/1/5 ratio (B) are shown in **Figure 2** as the typical heating thermograms. At this polymer ratio for the melted spun fibers, the crystallization traces of the minor component, PHB, for both thermograms are practically absent. Consequently the curves under PLA/PHB relations 1/0, 9/1, and 7/3 belong to the PLA as the dominant component. In **Table 1** the temperatures of thermal transfers are presented not only for loaded blends but for the pristine bio-based polymers (1/0 and 0/1) composing both the ultrathin fibers (f) and the corresponding films (s).

From the literature data as well as from the Table 1 it follows that PLA, PHB, and their blends have three principal thermal transitions which occur at the melting point, T_m, glass transition temperature, T_g, and cold crystallization, T_{cc}. Additionally, the crystallization temperatures obtained after heating are presented. The apparent melting temperatures for both bio-based polyesters loaded by 1% DPD differ in the limit of 5 degrees in Celsius scale and are equal to 170 and 175 °C for PLA and PHB fibers correspondingly as well as 173 and 178 °C for the analogous films. For the initial bio-based polymers without drug loading this discrepancy is higher and reaches 10 degrees Celsius. The decrease in the T_m with drug concentration is due to weak interaction between the drug functional groups and the ester bonds of the bio-based polymers probably via H-bonds formation likely.

The T_g values for PLA/PHB blends diverse in the range 40–60 °C and exceed markedly the respective value for PHB (≈10 °C) and remain constant or even slightly decrease with the drug content that could be explained by the drug-polymer interaction as well. Simultaneously, the noticeable rise of T_g for the blends and the pristine PLA fibers containing 1% DPD suggests that there is interaction between PLA and PHB segments as between polyester components partially compatible even without the introduction of special compatibilizers. It is worth to note that at the moderate crystallinity and higher (>40%) the T_g of PHB and PLA films could not be denoted by DSC measurements. Turning to the PLA/PHB comparison of the thermal behavior between the films and the fibers, it should be emphasis that for all of the PLA/PHB compositions, the crystallinity degree (see Table 1) of the films is higher than for melt electrospun fibers. During melt electrospinning, the polymer molecules oriented along the fiber axis have not enough time to rearrange their segmental conformations that are suitable for following crystallization. Comparing the principal thermophysical transition points,

Table 1. Comparative thermal characteristics of PLA/PHB blends in the form of ultrathin fibers (f) and films (s).

Polymer ratio PLA/PHB x% DPD	Melting, T_m °C	Glass transition, T_g °C	Crystal-lization, T_c °C	Cold crystal-lization, T_{cc} °C	Crystallinity degree, X_c, %
1:0 + 1% (f)	170	51	84	66	32
1:0 + 1% (s)	173	-	88	62	45
9:1 + 1% (f)	168	55	81	61	32
9:1 + 1% (s)	169	61	85	88	40
7:3 + 1% (f)	165	60	86	-	25
7:3 + 1% (s)	168	45	92	91	36
9:1 + 5% (f)	145[a)]	54	-	103	19
9:1 + 5% (s)	159	48	94	-	29
7:3 + 5% (f)	145	57	-	-	13
7:3 + 5% (s)	156	40	101	-	24
0:1 + 1% (f)	175	-	102	96.5	48
0:1 + 1% (s)	178	-	110	102	69

T_m and T_c are temperatures of melting and crystallization, respectively; T_{cc} and T_g are corresponding temperatures of cold crystallization and glassy-state transition; X_c is crystallinity degree. The averaged relative deviation of the temperature values is 3 and 5–6% for enthalpy data.
[a)] at 128 °C there is the second melting peak being not typical for the other systems.

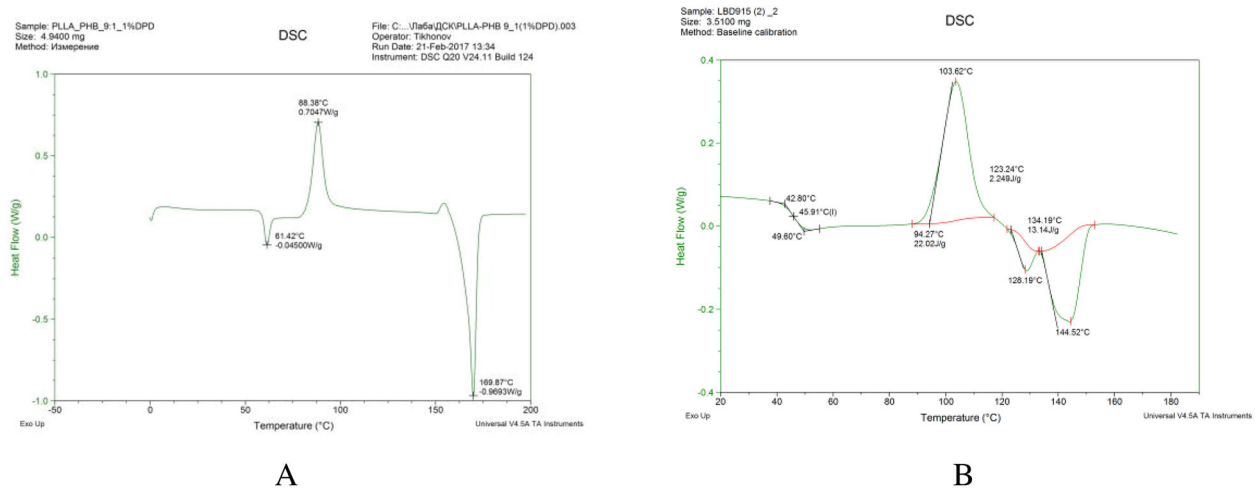

Figure 2. The typical DSC curves for PLA/PHB ultrathin fibers (A) and films (B) loaded with 1% and 5% DPD, respectively.

namely melting and crystallization temperatures for fibers and films, it could reveal that both processes occur at higher temperatures in the films. Besides, for both geometrical forms of bio-based polymers loaded by 1% DPD the supercooling degree, that is, the difference between T_m and T_c, is approximately equal within $\pm 2.5\,^{\circ}C$. The supercooling degree for the PLA/PHB film loaded by 5% DPD is $10\,^{\circ}C$ higher than for the ultrathin fiber of similar composition. As it was reported in the previous work,[9,18] the lowering in crystallization temperature reveals a faster crystallization rate of PLA in the blend fibers compared to that in pristine PLA fibers due to the ability of PHB to promote the recrystallization of PLA. However, after the increment of drug content from 1 to 5% the increase in this characteristic is observed as a result of drug impact upon segmental motion of the biopolymer. In more details the consideration of molecular mobility is represented in the next section.

3.3. Segmental Dynamics of Tempo Spin-Probe in the PLA/PHB Fibers and Films

In **Figure 3** there are typical ESR spectra of the TEMPO probe encapsulated in PLA, PHB and the PLA/PHB blend films (A) and fibrils (B), respectively. The spectral features of the PLA and PHB fibrillar samples are essentially distinguished. As it was represented in the previous section, the PLA/PHB fibers obtained via melt spinning have the lower degree of crystallinity relative to the analogous films. Hence, for the PLA-dominated fibers with high concentration of amorphous phase there is a well resolved triplet generated by the fast rotative mobility of the ESR probe (line 3B). The intermediate ratio PLA/PHB = 7/3 is characterized by the spectrum (line 2B) which presents the spectra superposition of two pristine polymers with the intrinsic time correlations τ_{PLA} and τ_{PHB}.

In contrast, the probe embedded in PLA/PHB films displays predominantly homogeneous rotation that becomes quite obvious in the comparison of the spectra (Figure 3A, lines 1–4). Additionally note that in the ultrathin fibers of PHB after melt electrospinning, the sharp increase in probe mobility is much more pronounced than that in PLA and its fibrillar blends. Taking into consideration the above results, this effect makes it possible to assume that the drug embedding leads to a small plasticizing effect related to not only with crystallinity decrease but with enhancing in segmental mobility in PHB. In contrast, for the PHB-containing fibers (Line 1 in **Figure 4**), where the latter presents as the dominant component, the drug plasticization is manifested most clearly. Except the τ_{PHB} value, for the other fibrillar systems the effective correlation times are weakly dependent on the drug concentration as well as on the PLA/PHB ratio (see Figure 4).

Nevertheless, the results of probe rotation dynamics, and hence the segmental mobility of the polymers, enable us to upbuild a series of the effective correlation times namely

$$\tau_{PLA} \approx \tau_{9:1} < \tau_{7:3} << \tau_{PHB}$$

Here the high crystalline biopolymer has probe rate rotation exceeding these characteristics for the other blend polymer systems and especially the pristine PLA.

3.4. Diffusion Impact on Drug Release From the PLA and PHB Ultrathin Fibers and Films

Figure 5 demonstrates the kinetic profiles of DPD release from the PLLA/PHB ultrathin fibers loaded by DPD and assembled in the mats collected during melt spinning. In comparison to the fibrillar mats, the analogous drug release curves are presented but for the melt-moulded bulk films. Both bio-based polymer systems display two specific ranges such as nonlinear and linear ones, the physical meaning of which has been recently analyzed for the analogous solution-electrospun ultrathin mats and the solution-cast bulk films.[19,20]

As can be seen from the figure, the curves belonging to the fibers are located below the corresponding curves for the films and the rates of release for them are remarkably lower. In accordance with the proposed diffusion-kinetic model,[9,21] the initial nonlinear section of each curve reflects principally the

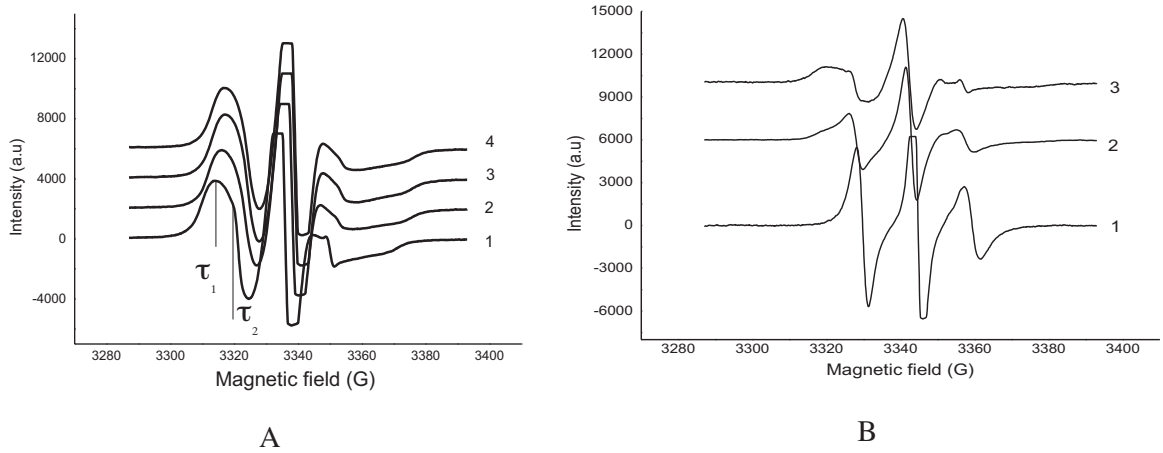

Figure 3. The family of spin-probe ESR spectra for films (A) and ultrathin fibers with different polymer content (B): A – PHB (1), PLA/PHB 9:1 (2), PLA/PHB 7:3 (3), and PLA (4); B – PLA (1), PLA/PHB 7:3 (2), and PHB (3).

drug diffusion process, whereas the linear section corresponds to the kinetic process of the surface hydrolytic fiber destruction with the corresponding loss in polymer weight strongly on the polymer surfaces. As a result of zero-order hydrolytic reaction, the immobilized fraction of the encapsulated drug releases from the cylindrical filaments and from fibrillar mat as the whole system at a constant rate. Thus, in any moment the drug concentration in a surrounding aqueous medium (e.g., a phosphate buffer) is the sum of mobile fraction transferring via diffusion mechanism and the immobilized fraction released via a zero-order kinetic mechanism as well.

In a PLA/PHB fibrillar mat prepared as a rectangular parallelepiped consisting of disordered entangled fibers, the drug effective diffusivity, D_{eff}, is determined by two consecutive processes such as diffusion in the inherent fiber volume with diffusivity, D_f, and the diffusion transport in the inter-fibrillar voids of the mat that are filled by an aqueous solvent (D_W).

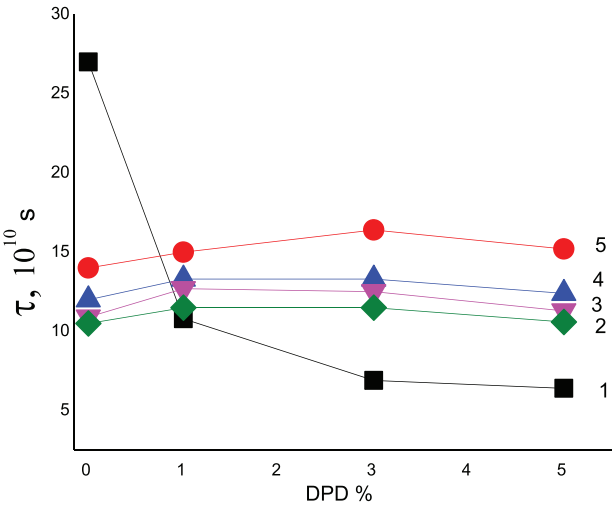

Figure 4. Dependence of effective correlation time on the drug (DPD) content in the fibers with different PLA/PHB ratio: 0/1 (1), 1/0 (2), 9/1 (3), 7/3 (4), and 6/4 (5).

Describing the two-stage diffusion as the drug transport in the quasi two-layer medium with two different diffusion coefficients, in accordance with the Crank's simplification,[22] D_{eff} can be presented as

$$L_M/(D_{eff}) = X_f/D_f + L_w/D_w \quad (1)$$

where X_f, L_w, and L_M are the averaged geometric characteristics of drug diffusion path in the fibers, the interfibrous voids, and the effective thickness of mats correspondingly.

For the cylindrical fibers, X_f is the fiber diameter, while for Lw, in accordance with the Mackie–Meares equation,[23] the correction for the increasing in the drug diffusion path due to the mat tortuosity was chosen as

$$\mathrm{Lw} = [(1+\varphi_f)/(1-\varphi_f)]^2 \mathrm{L_M}, \quad (2)$$

where ϕ_f is the volume fraction of polymer fibers in the mat. This correction was previously used to describe the drug diffusion in the PHB magnetic composites with the magnetite nanoparticles forming the extended aggregates.[24]

In a PLA/PHB fibrilar mat prepared as rectangular parallelepiped consisted of disordered entangled fibers, D_{eff} is determined by two consecutive processes such as the drug diffusion in the inherent fiber volume with diffusivity, D_f, and the drug diffusional transport in the interfibrillar space of the mat that is filled by aqueous solvent (D_W). Describing the two-stage diffusion as a drug transport in the quasi two-layer medium with two different diffusion coefficients in accordance with the Crank simplification,[23] the D_{eff} can be presented as

$$L_M/(D_{eff}) = X_f/D_f + L_w/D_w \quad (1)$$

where X_f, L_w, and L_M are the averaged geometric characteristics of drug diffusion path in the fibers, the interfibrous space, and the effective thickness of mats. For the cylindrical fibers, X_f is fiber diameter, while for L_w, in accordance with the Mackie–Mears equation,[24] the correction for increasing in the drug diffusion path was chosen as

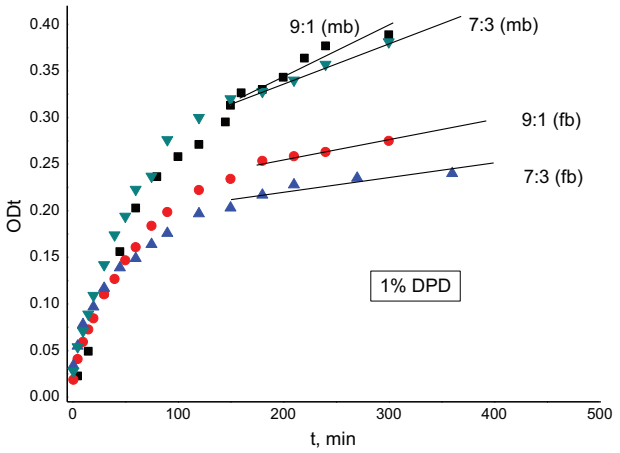

Figure 5. Comparison in the kinetic profiles of drug delivery (1% DPD) between the PLA/PHB blends prepared as the films (mb) and the ultrathin fibers (fb). The numbers at the curves show the proportion of blended components (PLA/PHB).

$$Lw = [(1 + \varphi_f)/(1 - \varphi_f)]L_M, \quad (2)$$

where ϕ_f is the volume fraction of polymer fibers. This correction was previously used to describe the drug diffusion in the PHB magnetic composites with the magnetite nanoparticles forming the extended aggregates.[25]

The differential equation of diffusion in the cylindrical fibers loaded with uniformly distributed drug was advanced by Crank:[23]

$$\partial C_D/\partial t = (1/r)D_f[\partial(r\partial C_D/\partial r)/\partial r] \quad (3)$$

$$\text{at } 0 < r < Xf/2, \quad (,)$$

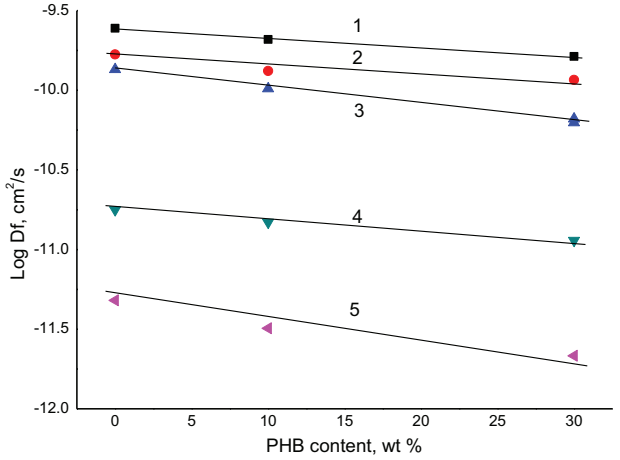

Figure 6. Semi-log dependence of DPD diffusivities on the polymer content (PHB concentration) in the films (1–3) and the ultrathin fibers (4,5) with diverse drug loading 1% (1,4), 3% (2,5), and wt 5% (3).

where r is the coordinate of the radial diffusion; symbol C_D, as in Equation (2), denotes the concentration of the mobile fraction of the drug in the cylindrical fiber with the corresponding constant diffusion coefficient D_f, and X_f is the average diameter of the fibers.

In accordance with the comprehensive research of Siepmann et al.,[26] the simplified solution of differential Equation (3) with corresponding initial and boundary conditions makes it possible to obtain the dependence of the cumulative amount of the on the time of release (t):

$$M_t/M_\infty = \left[16D_f/\pi X^2 f\right]^{1/2} t^{1/2} - \left[2D_f/X^2 f\right]t, \quad (4)$$

where M_∞ is the limiting value of M_t under the condition: $t \to \infty$.

For Equation (3) and its solution (4), which reflect the drug transfer through the surface of side walls in a cylinder, it is suggested that the cylindrical fiber length is higher than its radius by at least five times.[27] This mathematical requirement is fully fulfilled for the electrospun fibers with practically infinite length. Additionally, it is important to note that the latter equation should be valid under conditions $M_t/M_\infty \leq 0.4$. The expression for drug release from cylindrical fibers being subjected to polymer hydrolysis and drug diffusion simultaneously has the following form:

$$M_t/M_\infty = \left[16D_f/\pi X^2 f\right]^{1/2} t^{1/2} + k_c t, \quad (5)$$

here $k_c = k_h - [4D_f/X_f^2]$. The positive sign in the equation shows that for the PLLA/PHB fibers the inequality, $k_h > [4D_f/X_f^2]$, is fulfilled that was shown in the Figure 5. The experimental curves are consistent with Equation (5) that provides the way of drug diffusivity evaluation in the diffusion coordinates: $M_t/M_\infty \sim t^{1/2}$.

In the initial time interval $M_t/M_\infty \leq 0.5$, for rectangular films and slabs, the drug diffusion impact has the well-known expression[23]:

$$Mt/M_\infty = 8\left[D_s/\pi Xs^2\right]^{0.5} t^{0.5} \quad (6)$$

The comparison of drug diffusivities in the nanofiber mats and the macroscopic films with comparable thicknesses (about 80 μm) calculated by equations (5) and (6), respectively is represented in the semi-log forms in **Figure 6**. The evaluated data were obtained for variable biopolymer blend ratios and the various drug concentrations (1–5%).

In accordance with the above results showed in Figure 6, there are a big difference in drug diffusion coefficients for the films and the fibers if the other conditions being equal. The slow mobilities of drug molecules in melt-spun fibers could be attributed to both the heightened crystallinity degree and the sufficiently dense structure in the amorphous fields of fibrillar specimens. Besides, it is worth to note that the low values of D_f are in the satisfactory agreement with the same low values of the diffusion mobility of DPD in PHB microparticles.[28]

4. Conclusions

For the PLA/PHB blends loaded with drug content (1 and 5 wt%) prepared in the forms of macroscopic films and submicron fibers, surface morphology, crystallinity, thermal transition

temperatures, spin-probe segmental dynamics, and diffusion kinetics of drug release were compared to consider the distinction in their behaviors as the potential expectants designated for therapeutic design.

The increase in content of minor polymer component (PHB) depresses the PLA crystallinity degree and its crystallization temperature but for the ultrathin fibrils these effects are more pronounced. During film molding and fiber melt-electrospinning after blend polymer solidification, gained crystallization impact upon segmental dynamics in amorphous fields of the polymer that should tune the drug diffusivity and the corresponding release profile. The probe ESR spectroscopy data have shown that segmental dynamic homogeneity is more typical for the melted films, while the melt-spun fibers have the wide spectrum of TEMPO time correlations. The drug content in the blend fibers adjusts the segmental mobility relatively weak (see Figure 4) while the PLA/PHB blend ratio influences on the form of ESR spectra quite remarkably and hence modulates effectively the probe mobility in the fibers (Figure 3B).

In turn, the segmental mobility determines the drug diffusion that should lead to a diffusivity difference between the fibers and the films. Indeed, based on the correlation time values (τ), such difference must be within one or two orders of magnitude. In Figure 6 the diffusion data represented in the semilogarithmic coordinates confirm this discrepancy in diffusion coefficients satisfactory. The discovered differences in the segmental mobilities and drug diffusivities for both the films and the fibers could be explained as a result of modification of polymer chain conformations in the nanofibrile confined space.[29] The complex study of PLA/PHB fibers and films and subsequent features' comparison of the different geometrical forms will allow the experts to facilitate an understanding of reasonable diversification PLA/PHB of blend content for macro- and submicrone-sized drug delivery vehicles.

Acknowledgements

The paper was financially supported by the RF State Program of Fundamental Scientific Investigation RAN AAAA-A17-117040610309-0 as well as the National Natural Science Foundation of China (Grant Number 21374008). The authors gratefully acknowledge Dr. R. Kosenko (ICP Moscow) and Dr. E. Kucherenko (ICP Moscow) for drug release experiment performances.

Keywords

diffusion, drug release, PLA/PHB blends, melt-electrospun nanofibers, molded films

[1] S. Farah, D. G. Anderson, R. Langer, *Adv. Drug Del. Rev.* **2016**, *107*, 367.
[2] S. S. Patil, R. D. K Misra, *J. Mat. Technol. Adv. Perf. Mat.* **2018**, *33*, 364. https://doi.org/10.1080/10667857.2018.1447266
[3] B. D. Ulery, L. S. Nair, C. T. Laurencin, *J. Polymer Sci*. **2011**, *49*, 832. https://doi.org///10.1002/polb.22259
[4] G. G. D'Souza, V. Weissig, *Exp. Opin. Drug Delivery*. **2009**, *6*, 1135. https://doi.org/10.1016/j.ejphar.2013.01.075
[5] J. Zhang, E. I. Shishatskaya, T. G. Volova, L. Ferreira da Silvae, G.-Q Chen, *Mat. Sci. Eng. C* **2018**, https://doi.org/10.1016/j.msec.2017.12.035
[6] B. Tyler, D. Gullotti, A. Mangraviti, T. Utsuki, H. Brem, *Adv. Drug Delivery Rev.* **2016**, *107*, 163.
[7] J. Siepman, F. Siepman, *J. Contr. Rel*. **2012**, *161*, 351.
[8] N. A. Peppas, *Adv. Drug Delivery Rev.* **2013**, *65*, 5.
[9] K. Cao, Y. Liu, A. A. Olkhov, V. Siracusa, A. L. Iordanskii, *Drug Deliv. Transl. Res*. **2018**, *8*, 291. https://doi.org/10.1007/s13346-017-0463-7
[10] G Xie, Y Wang, X Han, Y Gong, J Wang, J Zhang, et al. *Ind. Eng. Chem. Res*. **2016**, *55*, 7116.
[11] M.P Arrieta, J López, D López, J.M Kenny, L. Peponi, *Eur. Polym. J*. **2015**, *73*, 433.
[12] A Repanas, B. Glasmacher, *J. Drug Deliv. Sci. Technol*. **2015**, *29*, 132. https://doi.org/10.1016/j.jddst.2015.07.001
[13] DE Budil, S Lee, S Saxena, JH. Freed, *J. Magn. Reson*. **1996**, *120*, 155.
[14] VP Timofeev, AY Misharin, YV. Tkachev, *Biophysics*. **2011**, *56*, 420.
[15] AL Buchachenko, AM. Vasserman, *In stable radicals*. Chemistry. RF, Moscow **1973**.
[16] A. P. Bonartsev, A. P. Boskhomedgiev, A. L. Iordanskii, et al. *Kinetics, catalysis and mechanism of chemical reactions. From pure to applied science. V.2 —Tomorrow and perspectives* (Eds.: R.M. Islamova, S.V. Kolesov, G.-E. Zaikov), Nova Science Publishers, New York **2012**, Ch.27. pp. 335.
[17] S. Megelski, J. S. Stephens, D. B. Chase, J. F. Rabolt, *Macromolecules* **2002**, *35*, 8456. https://doi.org/10.1021/ma020444a.
[18] T. Furukawa, H. Sato, R. Murakami, J. Zhang, Y. X. Duan, I. Noda, et al. *Macromolecules* **2005**, *38*, 6445. https://doi.org/10.1021/ma0504668
[19] S. G. Karpova, A. A. Ol'khov, N. G. Shilkina, A. A. Popov, A. G. Filatova, E. L. Kucherenko, A. L. Iordanskii, *Polym. Sci*. **2017**, *59*, 58.
[20] A. A. Olkhov, O. V. Staroverova, A. P. Bonartsev, I. I. Zharkova, E. D. Sklyanchuk, A. L. Iordanskii, S. Z. Rogovina, A. A. Berlin, A. A. Ishchenko, *Polym. Sci*. **2015**, *8*, 100.
[21] A. L. Iordanskii, A. A. Ol'khov, S. G. Karpova, E. L. Kucherenko, R. Yu. Kosenko, S. Z. Rogovina, A. E. Chalykh, A. A. Berlin, *Polymer Sci*. **2017**, *59*, 343. https://doi.org/10.1134/S0965545×17030075
[22] J. Crank, *The mathematics of diffusion*, 2nd ed., Clarendon Press, Oxford **1975**.
[23] J.S Mackie, P. Meares, *Theoretical. Proc. R Soc. Lond*. **1955**, *232*, 498. https://doi.org/10.1098/rspa.1955.0234
[24] A.V Bychkova, A.L Iordanskii, A.L Kovarski, O.N Sorokina, RY Kosenko, VS Markin, et al. Magnetic and transport properties of magneto-anisotropic nanocomposites for controlled drug delivery, *Nanotechnol. Russ*. **2015**, *3-4*, 325. https://doi.org/10.1134/S199507801502007X
[25] J Siepmann, F. Siepmann, *Int. J. Pharm*. **2008**, *364*, 328. https://doi.org/10.1016/j.ijpharm.2008.09.004
[26] B. Jämstorr, *Acta Univ. Ups. Abstr. Uppsala Diss. Fac. Sci. Technol*. **2016**, *884*.
[27] A. L. Iordanskii, S. Z. Rogovina, R. Yu. Kosenko, E. L. Ivantsova, E. V. Prut, *Dokl. Phys. Chem*. **2010**, *431*, 60. https://doi.org/10.1134/S0012501610040020
[28] A. P. Bonartsev, V.A Livshits, T.A Makhina, V.L Myshkina, G. A Bonartseva, A. L Iordanskii, *Express Polym Lett*. **2007**, *1*, 797. https://doi.org/10.3144/expresspolymlett.2007.110
[29] R. L. Jones, S. K. Kumar, D. L. Ho, R. M. Briber, T. P. Russell, *Macromolecules* **2001**, *34*, 559. https://doi.org/10.1021/ma001141o

